A hydrogel-based *in vitro* assay for the fast prediction of antibiotic accumulation in Gram-negative bacteria

Robert Richter [a,b], Mohamed.A.M. Kamal [a], Mariel A. García-Rivera [c], Jerome Kaspar [d], Maximilian Junk [d], Walid A.M. Elgaher [a], Sanjay Kumar Srikakulam [a], Alexander Gress [a], Anja Beckmann [e], Alexander Grißmer [e], Carola Meier [e], Michael Vielhaber [d], Olga Kalinina [a,f], Anna K.H. Hirsch [a,b], Rolf W. Hartmann [a], Mark Brönstrup [c,g], Nicole Schneider-Daum [a], Claus-Michael Lehr [a,b,*]

[a] Helmholtz Institute for Pharmaceutical Research Saarland (HIPS) – Helmholtz Centre for Infection Research (HZI), 66123 Saarbrücken, Germany
[b] Department of Pharmacy, Saarland University, 66123 Saarbrücken, Germany
[c] Department of Chemical Biology, Helmholtz Centre for Infection Research (HZI), 38124 Braunschweig, Germany
[d] Institute of Engineering Design, Saarland University, 66123 Saarbrücken, Germany
[e] Department of Anatomy and Cell Biology, Saarland University, 66421 Homburg, Germany
[f] Medical Faculty, Saarland University, 66421 Homburg, Germany
[g] German Centre for Infection Research (DZIF), 38124 Braunschweig, Germany

ABSTRACT

The pipeline of antibiotics has been for decades on an alarmingly low level. Considering the steadily emerging antibiotic resistance, novel tools are needed for early and easy identification of effective anti-infective compounds. In Gram-negative bacteria, the uptake of anti-infectives is especially limited. We here present a surprisingly simple *in vitro* model of the Gram-negative bacterial envelope, based on 20% (w/v) potato starch gel, printed on polycarbonate 96-well filter membranes. Rapid permeability measurements across this polysaccharide hydrogel allowed to correctly predict either high or low accumulation for all 16 tested anti-infectives in living *Escherichia coli*. Freeze-fracture TEM supports that the macromolecular network structure of the starch hydrogel may represent a useful surrogate of the Gram-negative bacterial envelope. A random forest analysis of *in vitro* data revealed molecular mass, minimum projection area, and rigidity as the most critical physicochemical parameters for hydrogel permeability, in agreement with reported structural features needed for uptake into Gram-negative bacteria. Correlating our dataset of 27 antibiotics from different structural classes to reported MIC values of nine clinically relevant pathogens allowed to distinguish active from nonactive compounds based on their low *in vitro* permeability specifically for Gram-negatives. The model may help to identify poorly permeable antimicrobial candidates before testing them on living bacteria.

Introduction

Since their "Golden Age" (1930s to 1960s), the number of novel antibiotics has been steadily decreasing [1,2], while bacterial resistance is continuously increasing [3]. Especially, infections caused by Gram-negative bacteria are about to lack appropriate treatment, because the pipeline of new anti-infective compounds is only poorly filled [4]. While the limited profitability of antibiotic research is one crucial factor for this crisis, a further one is the low accumulation of antibiotics inside

Gram-negative bacteria. The main cause for this is the Gram-negative cell envelope, which has been neglected in antibiotic drug discovery for a long time [5]. The elements of the biological barrier (Fig. 1) and their efficacy in limiting the accumulation of antibiotics, however, are increasingly understood [6–13]. One can expect that drug accumulation in Gram-negative bacteria is mainly governed by compound uptake and efflux [14]. Lately, different research groups concluded that the extent of passive uptake through porins can determine if a drug accumulates high or low [15–17]. Indeed, the major antibiotic classes used against Gram-negative infections, such as β-lactams, tetracyclines,

---

Abbreviations

%IncMSE	relative increase of mean squared error in %
AMP	ampicillin
AZT	aztreonam
Caco-2	cell line consisting of heterogeneous human epithelial colorectal adenocarcinoma cells
CEF	cefuroxime
CHL	chloramphenicol
CIP	ciprofloxacin
CLI	clindamycin
clogDpH7.4	calculated common logarithm of distribution coefficient at pH 7.4
CLSM	confocal laser scanning microscopy
ERY	erythromycin
FUS	fusidic acid
HPLC	high performance liquid chromatography
IMI	imipenem
KAN	kanamycin
LC	liquid chromatography
LEV	levofloxacin
LIN	lincomycin
magn	magnification
MIC	minimum inhibitory concentration
MIN	minocycline
NAL	nalidixic acid
NOR	norfloxacin
NOV	novobiocin
Omp	outer membrane protein
PAMPA	parallel artificial membrane permeation assay
Papp	apparent permeability coefficient
PIP	pipemidic acid
resp	respectively
RF	random forest analysis
RIF	rifampicin
RNAP	ribonucleic acid polymerase
SE	standard error of the mean
SPA	Sparfloxacin: spp.species (pl.)
STR	streptomycin
SUL	sulfamethoxazole
TET	tetracycline
TIG	tigecycline
TOB	tobramycin
VAN	vancomycin

fluoroquinolones, and some aminoglycosides access Gram-negative bacteria mainly through porins [6,11,18,19]. Porins are protein channels and versatile in structure. They can appear as trimers or monomers, can have diameters as large as 1.5 nm or as small as 0.6 nm and can feature different sequences of amino acids facing the inner of the channel and thus lead to different compound selectivity [20]. Very well-studied porins are those of *Enterobacteriaceae*, such as *Escherichia coli*, *Salmonella enterica* or *Klebsiella pneumoniae*. It is known that these species predominantly feature so-called fast and rather nonspecific porins, as for example, OmpF, OmpC (*E. coli, S. enterica*), and OmpK35 (*K. pneumoniae*) [6].

Several *in vitro* assays such as liposome [21] or outer-membrane-vesicle swelling assays [22], assays based on reconstituted vesicles [23], and electrophysiological studies [24–26] have been developed to better understand this entry route. Further important

assays exist using living bacteria [27–30]. Moreover, several *in silico* simulations of drug transport across porins have been employed [31–34]. These assays helped to conclude that molecular size, shape, flexibility, polarity, certain functional groups, and charge of the permeating compound seem to determine permeation through these outer membrane proteins [17,35–38].

While Caco-2 cell-based or cell-free Parallel Artificial Membrane Permeability Assays (PAMPA) are already established to predict intestinal drug uptake into humans [39,40], this is not yet the case for analogous assays for studying uptake into bacteria. This may be because of issues regarding work-place safety, time consumption, relatively high costs, and/or low-throughput capacity [41]. In the context of antibiotic permeability testing, hydrogels have so far only been considered as a nonfunctional and rather structural building block [42]. Yet, they are
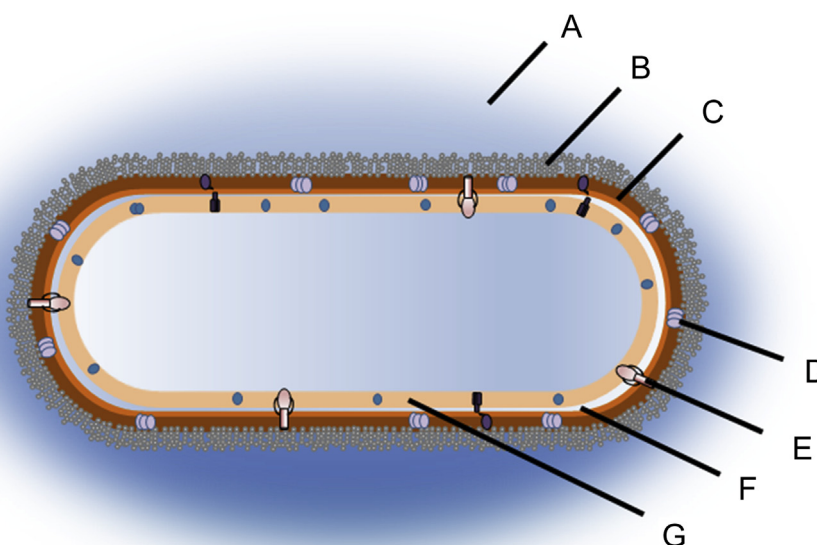

Fig. 1. Permeation barriers of Gram-negative bacteria. (A) Biofilm (optional), (B) lipopolysaccharide-rich outer leaflet of outer membrane, (C) phospholipid-rich inner leaflet of the outer membrane, (D) porin, (E) multidrug efflux pump, (F) periplasmic space, (G) Plasma membrane.

highly versatile in their properties, adjustable in their gel network density, and often come along with low material costs. Hence, they would be potentially suitable materials to mimic this process and constitute a valuable tool for the current challenges of antibiotic drug discovery against Gram-negative bacteria. The importance of natural hydrogels such as mucus and bacterial biofilms to limit the access of antibiotics to their targets has already been pointed out by the work of Ribbeck et al. [43,44]. Moreover, polysaccharide hydrogels are also essential components for a wide range of analytical methods and applications, such as size exclusion chromatography and gel electrophoresis [45–47]. This led us to the hypothesis that polysaccharide gels may feature fundamental separation criteria relevant also for the permeability of compounds across the Gram-negative bacterial cell envelope and that such permeability data could be used for predicting antibiotic accumulation in such bacteria.

As a result, we here present a 96 well-based, relatively simple, quick, and cost-effective assay to measure permeability across a starch-based membrane surrogate of the Gram-negative bacterial cell envelope. In spite of its simplicity, this assay shows surprisingly high accuracy in predicting bacterial accumulation, qualifying it as a useful tool for optimizing the passive transport of anti-infective compounds across this important biological barrier and for excluding many inactive compounds already at an early stage of antimicrobial drug development.

Materials and methods

Materials

MultiScreen® 96-well Filter plates with 0.4 μm PCTE membrane and MultiScreen® 96-well Transport Receiver Plates were obtained from EMD Millipore Corporation (Billerica, Ma, USA). Sodium alginate (Propanal LF 10/60 FT) was obtained from FMC Biopolymer UK Ltd. (Girvan, Ayrshire, UK). Amylopectin (ELIANE 100) and potato starch (Partially hydrolyzed, M_w > 1.500 kDa, amylose content 33%) were donated by AVEBE U.A. (Veendam, NE). Agarose SERVA and Streptomycin-SO_4 (both research grade) were obtained from SERVA Electrophoresis GmbH (Heidelberg, Germany). Ampicillin-Na (CELLPURE®, purity ≥91%) was obtained from Carl Roth GmbH + Co. KG (Karlsruhe, Germany). Aztreonam (96.5%, research grade) was obtained from MP Biomedicals, LLC (Illkirch, France). Tetracycline-HCl (>99%) was obtained from chemodex (St. Gallen, Switzerland). Rifampicin (molecular biology grade, purity ≥90%) was obtained from USBiological (Swampscott, MA, USA). Tigecycline (purity >97%) and pipemidic acid (purity ≥98%) were obtained from LKT Laboratories, Inc. (St. Paul, MN, USA). Imipenem (purity ≥98%) was obtained from MOLEKULA® GmbH (Munich, Germany). Amylose (research grade), novobiocin sodium (purity ≥95%) and sulfamethoxazole (purity ≥98%) were purchased from Cayman Chemical Company (Ann Arbor, MI, USA). Phosphate buffered saline (PBS, pH 7.4) was prepared from dissolution of 0.02 M PBS tablets without potassium (Genaxxon Bioscience, Ulm, Germany) in 1 L of Milli-Q water. Hydrochloric acid and sodium hydroxide solutions (1 M each) were used from Bernd Kraft (Duisburg, Germany). Methanol, acetonitrile (both HPLC grade), acetic acid (glacial) were obtained from VWR Chemicals (VWR International S.A.S., Fontenay-sous-Bois, France). Methylene blue was obtained from J.T. Baker (Avantor™ Performance Materials, Radnor, PA, USA). Fluoraldehyde™ (o-phthaldialdehyde reagent solution) was obtained from Thermo Fisher Scientific (Waltham, MA, USA). Chitosan (high molecular weight), tobramycin (purity ≥90%), kanamycin monosulfate (purity ≥75%), erythromycin (purity 98%, research grade), ciprofloxacin (purity ≥98%, HPLC grade), chloramphenicol (purity ≥98%, HPLC grade), nalidixic acid (purity ≥98%) norfloxacin (≥98%, analytical standard), minocycline hydrochloride (technical grade one, purity 100%), sparfloxacin (purity ≥99%, HPLC grade), fusidic acid sodium (≥98%, TLC grade), levofloxacin (purity ≥99%, HPLC grade), clindamycin hydrochloride (≥96%, TLC grade), lincomycin hydrochloride (Pharmaceutical secondary standard),

cefuroxime sodium (analytical standard) were obtained from Sigma-Aldrich Co. (St. Louis, MO, USA).

Methods

Membrane preparation

Due to differences in the viscoelastic properties of the employed polysaccharide gels, concentrations varied between the different polysaccharides. Alginate gels of 5%, 10%, 15%, and 20% (w/v) were made by adding respective amounts of Propanal LF 10/60 FT to a falcon tube filled with 30 mL of Milli-Q water at room temperature. Immediately thereafter, the tube was closed and intensely shaken for 1 min. The suspension was kept overnight inside a 70 °C water bath to allow for complete dissolution. For 3% (w/v) chitosan gel 300 mg high molecular mass chitosan were dissolved overnight in 10 mL acetic acid (1% v/v). sodium hydroxide solution of 0.02 M concentration was optionally given for neutralization (pH 7.4). For 2.5%, 5%, 7.5%, and 10% (w/v) agarose gels, the respective amount of agarose was suspended in 10 mL Milli-Q water and heated in the microwave for 1 min at 600 W. For 10%, 15%, 20%, 25%, 30%, and 35% (w/v) starch gels; 10%, 15%, 20%, and 25% (w/v) amylopectin, as well as 30%, 40%, 50%, and 60% (w/v) amylose, slightly acid degraded potato starch, amylopectin or amylose, respectively, were suspended in 10 mL of Milli-Q water and boiled until a clear solution formed. A displacement pipette (Transferpettor®, Brand GmbH & CoKG, Wertheim, Germany) was used to coat each filter support of MultiScreen® 96-well filter plates with 40 μL of the respective polysaccharide formulation. The covered and coated filter plates were kept overnight at 4 °C.

Preparation of donor solutions

Donor solutions of 100 μg/mL of rifampicin, novobiocin, tetracycline, clindamycin, and chloramphenicol were prepared by direct dissolution of the compounds in PBS (pH 7.4). The 100 μg/mL solutions of quinolones and nalidixic acid were prepared by dissolving 1 mg of compound in 1 mL of 0.1 M sodium hydroxide solution, adding 4 mL of PBS (pH 7.4), neutralizing the solution with 1 M hydrochloric acid and filling up to 10 mL by PBS (pH 7.4).

Hydrogel-based in vitro permeability assay

Assays were performed using the hydrogel-coated donor wells of 96-well filter plates in combination with a 96-well receiver plate. After equilibration of the hydrogel coatings from both sides in PBS (pH 7.4) at 37 °C for 30 min, PBS was removed and 230 μL prewarmed antibiotic donor solution (37 °C) were given into the respective donor wells, while 30 μL were immediately removed and diluted 1:10 in an extra plate. Corresponding wells of the receiver plate were given 300 μL of fresh PBS (pH 7.4). Donor and acceptor plate were reassembled, sealed with adhesive foil, and incubated (37 °C, 180 rpm). At 0, 10, 20, 30, 45, 60, 90, 120, 150, 180, 210, and 240 min, the transport system was disassembled to measure the absorbance in the acceptor wells of the receiver plate using a Tecan Infinite® 200 PRO (Tecan Trading AG, Mannedorf, Switzerland) plate reader. An adjusted protocol was followed for substances with insufficient absorbance. In case of tobramycin and kanamycin, samples of 20 μL were drawn and a quick fluorimetric approach was followed by diluting samples 1:11 by Fluoraldehyde™. The removed volume was replaced using fresh PBS (pH 7.4). In the case of other substances with insufficient absorbance signal, 220 μL of donor solution were given in each donor well; 20 μL were immediately removed and diluted 1:10. At all time points, samples of 40 μL were drawn from acceptor wells and diluted 1:5 for liquid chromatography coupled mass spectrometry (LC–MS). Permeated amounts of each compound were calculated in reference to calibration curves, which were prepared from the applied donor solution.

Quantification by UV-spectroscopy. At selected time points, the antibiotic

concentration in the receiver plates was directly quantified using a Tecan Infinite® 200 PRO plate reader, run by Tecan i-control, 1.10.4.0 software (Tecan Trading AG, Mannedorf, Switzerland). Antibiotics and absorbance wavelengths used for their quantification are listed in Table S1.

Quantification by fluorimetry. After reaction with Fluoraldehyde™, fluorescence was measured ($\lambda_{ex} = 360$ nm, $\lambda_{em} = 470$ nm) using a Tecan Infinite® 200 PRO plate reader and Tecan i-control, 1.10.4.0 software (both Tecan Trading AG).

Quantification by LC–MS/MS

An Accela UHPLC system coupled TSQ Quantum Access Max tandem quadrupole mass spectrometer (both from Thermo Fisher Scientific, Waltham, MA, USA) was used. The UHPLC device featured a quaternary mixing pump, an online degasser and a column oven. The entire system was operated via the standard software Xcalibur™ (Thermo Fisher Scientific, Waltham, MA, USA). Streptomycin samples were quantified using a Synchronis HILIC column (50 × 2.1 mm, 1.7 μm, Thermo Fisher Scientific) column. For all other compounds, an Accucore RP-MS column (150 × 2.1, 2.6 μm, Thermo Fisher Scientific, Waltham, MA, USA) was employed. The chromatographic analysis was performed with a binary solvent mixture using optionally acetonitrile + 0.1% formic acid (A), MilliQ-Water + 0.1% formic acid (B), methanol + 0.1% formic acid (C) or ammonium formate buffer (10 mM, pH 3, D). Ampicillin and sulfamethoxazole were analysed using an isocratic run with 60% B and 40% C or 40% A and 60% B, respectively. All other compounds followed a gradient run. As for clindamycin and lincomycin, the initial value of 18% A and 72% D was shifted to 30% A and 70% D within 2 min and then kept constant for another 2 min. As for tobramycin and streptomycin, the ratio of 95% A and 5% B was shifted after 2 min to 5% A and 95% B within 1.5 min, and then was kept constant for 3.5 min. Vancomycin samples were run for the first minute with 5% A and 95% B before shifting within 1 min to 95% A and 5% B and keeping the values for 3 min. Erythromycin was run starting with an immediate shift from 18% A and 82% D to 90% A and 10% D within 2 min. The latter ratio was kept constant for 3 min. Fusidic acid started with 35% B and 65% C. After 2 min, the values changed to 5% B and 95% C within 1 min. After that, these values were kept constant for 4 min. The detection of the compounds in the MS happened after heated electrospray ionization (H-ESI) during positive ion mode using for sulfamethoxazole single ion monitoring (SIM) and for all other selective reaction monitoring (SRM). LC–MS/MS parameters are summarized in Table S2.

Calculation of the apparent permeability coefficient (P_{app})

The slope was calculated from a linear cumulative permeation-time plot, at which the drug concentration did not yet exceed 10% of the apical compound concentration and at which no lag time occured. This slope was divided by the surface area A of the filter support (cm^2), to obtain the compound flux (J, μg/cm^2*s). P_{app} was then calculated using the following formula:

$$P_{app}\left(cm * s^{-1}\right) = \frac{J}{c_0}$$

where c_0 is the initial donor concentration (μg/cm^3).

Validation of starch-based permeability assay

Transport studies carried out for assay validation were performed under a reduced number of time points (10, 20, 30, 45, 60 and 90 min) and antibiotic donor solutions had a concentration of 200 μM. Since not all curves showed linear permeation behavior between 10 and 30 min, the area under the curve ($AUC_{10–30\ min}$) was calculated by integrating the permeation-time curves within the limits of 10–30 min.

Application of starch-based permeability assay on RNAP-inhibitors

Permeation studies on previously reported in-house RNAP inhibitors 1–3 [48] were carried out as mentioned under "*in vitro* permeability assay." The absorbance in the receiver plate was measured at time points 10, 20, 30, 45, 60 and 90 min. The initial donor concentration was 100 μM for each compound.

Printing of membranes

A customized 3D-printer was designed based on modular aluminum construction profiles with controls based on a Duet 2 32 Bit 3D-printer controller running a customized version of RepRapFirmware 2.02. The printer features igus® SHT spindle drive linear axes fitted with igus® MOT-AN-S-060-020-056-L-A-AAAA motors (both igus® GmbH, Cologne, Germany) for x/y/z motion with a resolution of 5 μm ± 5% and theoretical microstepped resolution of up to 0.625 μm. Extrusion of the starch solution is accomplished by a 10 mL Hamilton® SaltLine reagent syringe (model 1010 TLL-SAL, Hamilton® Company, Reno, NV, USA) driven by a Nanotec L4118S1404-M6X1 Hybrid linear actuator (Nanotec Electronic GmbH & Co. KG, Feldkirchen, Germany; full-step volume resolution of the driven syringe 0.837 μL per step). The syringe was kept at 80 °C by a VWR® refrigerated circulating bath with a digital temperature controller (model 1166D, VWR® International, LLC., Radnor, PA, USA). The hot water supply for the syringe consisted of a Masterflex L/S® easy-load® peristaltic pump (Cole-Parmer, Vernon Hills, IL, USA) adjusted to speed 1 and OMNILAB silicone tubing (5 × 2 × 9 mm, OMNILAB-LABORZENTRUM GmbH & Co. KG, Bremen, Germany) as well as PhthalateFree® PVC Pump Tubes (3.18 mm ID, Gilson® Company Inc., Lewis Center, OH, USA). A trimmed Sterican® needle for special indications (G 14 × 3 1/8"/Ø 2.10 × 80 mm, B. Braun Melsungen AG, Melsungen, Germany) was used as a nozzle. The g-code used to print the starch solution into the donor wells can be found in the supplementary information.

Absorbance scan of membranes and quantitative structural comparisons

As a quick check for batch homogeneity and evenness, 20% (w/v) starch solutions were prepared in 100 μg/mL methylene blue solution before coating the filter membrane. After coating, filter plates underwent an absorbance analysis using the Tecan Infinite® 200 PRO plate reader, with Tecan i-control, 1.10.4.0 software (Tecan Trading AG, Mannedorf, Switzerland). The scan was done at 666 nm (bandwidth 9 nm), using 15 × 15 reads/well with 25 flashes/read, no settle time and a border of 850 nm. As plate type, 'Millipore MultiScreen 96 Flat Bottom Transparent Polysterol' was selected. The obtained absorbance values per well were aligned in x and y direction and subsequently plotted as a 3D surface diagram using Microsoft® Excel® for Microsoft 365 MSO (16.0.12827.20200), Microsoft® Corp., Redmond, WA, USA).

Quantitative assessment of hydrogel coating

Hydrogel deposition was evaluated by calculating the average absorbance per membrane using the absorbance data of 177 points of nine wells and calculating the overall mean. The intra-well variability is represented by the mean standard deviation of all performed coatings. Regarding the intra-batch variability, the standard deviation of the mean absorbance of each coated well was averaged for each batch before calculating the mean of the obtained values. The inter-batch variability was obtained by calculating the standard deviation of the mean absorbance from each batch. Obtained data originate from at least 3 batches of membranes consisting of at least triplicates.

Transmission electron microscopy (TEM) of freeze-fracture replicas

For the analysis of the polysaccharide gels in TEM, starch hydrogels were prepared by dissolving modified potato starch in water (final concentrations were 10% or 20% or 40% (w/v)). Hydrogels of 10% agarose, 20% amylopectin and 30% amylose (w/v) were prepared in water too. The solutions were dropped onto glass cover slips and kept in the refrigerator for solidification. 24 h later, small slices of the hardened hydrogel were cut with a scalpel. The slices were incubated with phosphate-buffered saline (PBS) for 30 min at 37 °C and 5% CO_2. Thereafter, small pieces of the

hydrogel slices were mounted in between a sandwich of copper carriers (one flat-bottom, one with depression) and plunge-frozen into a nitrogen-cooled liquid ethane–propane mixture using the Leica plunge freezer EM CPC (Leica Microsystems, Wetzlar, Germany).

Afterwards, the sandwich carriers were mounted in a cryo-preparation box onto a nitrogen-cooled finger replica table and transferred with an EM VCT shuttle into the EM BAF060 freeze-fracture and etching device (all devices from Leica Microsystems). Freeze-fracturing was performed at -162 °C and 1×10^{-7} mbar by chipping off the upper copper carrier. Fractured samples were etched for 5 min at -100 °C. The etched surfaces were rotary shadowed with a 1.5 nm platinum-carbon coating applied at a 60° angle, followed by a 20 nm carbon coating applied at 90°. The replicas were stabilized on a gold index grid using 0.5% Lexan polycarbonate plastic dissolved in dichloroethane (DCE). After evaporating the DCE by incubating the sample-replica-Lexan-grid at -20 °C for 16 h, the samples were thawed at room temperature and the carriers were removed. Grids were given into 70% sulfuric acid for 3 h to dissolve the starch from the replicas. Afterwards, grids were given into double-distilled water for 1 h. The grids were dried on filter sheets and a 20 nm carbon coating was applied at 90° for further stabilization. After removal of the Lexan film by incubation in hot DCE, the analysis was performed using a FEI Technai G2 transmission electron microscope (FEI, Thermo-Fisher Scientific, Munich, Germany) at 100 kV, equipped with a digital 8-bit camera. The negative contrast was reversed for image interpretation, so that the heavy metal appears white and the shadow appears black.

In bacterio control assay

Bacterial uptake. A lysogeny broth (LB) of 5 ml was inoculated with *E. coli* MG1655 and incubated overnight at 37 °C and 150 rpm. 2×60 mL of fresh LB were inoculated with 1 mL of overnight culture (starting $OD_{600} \approx 0.1$) and incubated (37 °C, 150 rpm) till reaching $OD_{600} = 0.7$. The bacterial culture was centrifuged in 50 mL Falcon tubes (9 min, $4500 \times g$, 20 °C), the supernatant was removed and following resuspension of the pellet in 5 mL NaPi-MgCl$_2$ buffer (50 mM sodium phosphate (NaPi) + 5 mM MgCl$_2$ adjusted to pH 7.0, sterile filtrated) the suspension was centrifuged under the same conditions. Again, the supernatant was discarded, and the pellet resuspended in warm NaPi buffer to reach $OD_{600} = 5.0$. The obtained suspension was kept at 37 °C for 5 min. A bacterial suspension of 100 μL/well was given into a Multi-ScreenHTS DV filter plate (transparent, pore size 0.45 μm, Merck Millipore, Tullagreen, IRL) wetted with 2 μL NaPi buffer. At time points 0, 2, 5, 10, 20, 30, 42, 47, 50 and 52 min, 25 μL of the respective antibiotic solution was added and mixed in the corresponding wells to give a final concentration of 200 μM. The filter plate was shaken at 350 rpm and 37 °C in a ThermoMixer® C (Eppendorf GmbH, Hamburg, Germany) during antibiotic addition. For the 0 min time point, 25 μL of antibiotic solution were added right before filtration. The incubation was stopped at the respective time point by removal of the supernatant with a vacuum manifold (~15 s) and washing the cells twice with 100 μL of ice-cold NaPi buffer by a Bravo Automated Liquid-Handling Platform (Agilent Technologies, Santa Clara, CA, USA) and filtered again. The filter plate was pressed against absorbent paper to remove the remaining liquid after every filtration. The filter plate was put on top of a 350 μL conical bottom receiver plate (clear polypropylene, Greiner Bio-One GmbH, Frickenhausen, Germany) and pellets were resuspended in 100 μL of ice-cold methanol-water blend (8:2). After that, the suspension was incubated for 30 min at RT and 400 rpm while being sealed with Parafilm® (Bemis Company Inc., Neenah, WI, USA) and closed with a lid. Following the incubation step, the filter plate was centrifuged at $2250 \times g$ for 5 min and the filtrate collected in the receiver plate. The cell debris was further lysed by adding 100 μL of ice-cold acetonitrile to the filtrate and mixing before it was incubated for 30 min at RT and 400 rpm. Further centrifugation at $2250 \times g$ for 15 min and collection of filtrate was then followed by evaporation using a centrifugal vacuum concentrator at 20 °C

coupled to a cold trap at -50 °C (both from Labconco Corporation, Kansas, MO, USA). The dry remnants were reconstituted in 100 μL of a methanol-acetonitrile blend containing 0.1% formic acid and 10 ng/mL caffeine as internal standard, with the exception of streptomycin and tobramycin, which were reconstituted in 100 μL of water containing 0.1% formic acid and 10 ng/mL caffeine. Samples were subsequently measured by LC–MS/MS (see below). To determine the unspecific binding of the tested compounds, 100 μL of NaPi buffer were added to a blank filter plate and incubated for 5 min at 37 °C A compound of 25 μL from stock solutions was added and mixed as mentioned before. The plate was incubated until the 52 min time point and, from then on, treated like the bacteria-containing plate. The amount of antibiotic in bacterial samples was determined based on a corresponding regression curve. To calculate the effective accumulated amount obtained, the amount of corresponding compound in nmol from unspecific binding was subtracted from all data obtained from bacterial incubation.

Quantification of uptake by LC–MS/MS

Samples were quantified by an Agilent 1290 UHPLC (Agilent Technologies, Santa Clara, CA, USA) coupled to an AB Sciex QTrap 6500 ESI-QQQ (AB Sciex Germany GmbH, Darmstadt, Germany) mass spectrometer. For chromatographic separation, a ZORBAX Eclipse Plus C18 (2.1×5.0, 1.8 μm, Agilent Technologies, Santa Clara, CA, USA) column was employed. A linear gradient was applied using water $+0.1\%$ formic acid (A) and acetonitrile $+ 0.1\%$ formic acid (B), in which the initial amount 99% A shifted to 1% A over a period of 5 min and at a flow rate of 0.7 mL/min. Chromatographic separation of tobramycin samples was carried out in a Shodex HILICpak VC-50 2D column (20×150 mm, 5 μm, Showa Denko America Inc., NY, USA). A linear gradient was applied using water $+$ 1.5% ammonia (A) $+$ and acetonitrile 0.1% formic acid, starting at 70% A and reaching 90% A over a period of 5 min and at a flow rate of 0.3 mL/min. LC–MS/MS parameters are summarized in Table S3.

Minimum inhibitory concentration (MIC) determination

MIC values of CIP, NOV and compounds **1**–**3** were assessed as described previously with a slight modification [49]. Antibacterial activities against *Staphylococcus aureus* subsp. *aureus* (Newman strain), and *E. coli* TolC were determined in 96-well plates (Sarstedt, Nümbrecht, Germany). Bacterial cells were inoculated into lysogeny broth (LB) medium containing the compounds dissolved in PBS or DMSO (1% maximum concentration) to reach a total volume of 200 μL with an optical density at 600 nm (OD_{600}) of 0.03. Six concentrations of the test compounds were prepared (in duplicates) by twofold serial dilution. The ODs were measured using a PHERAstar Microplate reader (BMG labtech, Ortenberg, Germany) after inoculation (0 h) and after incubation at 37 °C with shaking at 50 rpm for 18 h. Given MIC values are means of two independent determinations and defined as the lowest concentration of compound that reduced OD_{600} by $\geq 95\%$. Percent inhibition of bacterial growth was calculated when less than 95% inhibition of bacterial growth was observed at the highest concentration.

Random forest analysis

The random forest model was created using randomforest library [50] in R (v. 3.6.1; R Core Team, R Foundation for Statistical Computing; 2017, Vienna, Austria). The input data ($AUC_{10–30 \ min}$, net charge, molecular mass, minimum projection area, relative abundance of unsaturated bonds, number of rotatable bonds, number of hydrogen bond acceptors, number of hydrogen bond donors, globularity, $clogD_{pH7.4}$) was initially processed and stored as a table. We used leave-one-out cross-validation to develop this model with the hyperparameters ntree of 100, mtry of 2 and maxnodes of 8. Where ntree is the number of decision trees we allow this model to grow, mtry is the number of variables randomly sampled at each split or tree node and maxnodes is the maximum number of terminal nodes every tree in the forest can have. The depth of the tree can be controlled using the maxnodes hyperparameter. In the process of
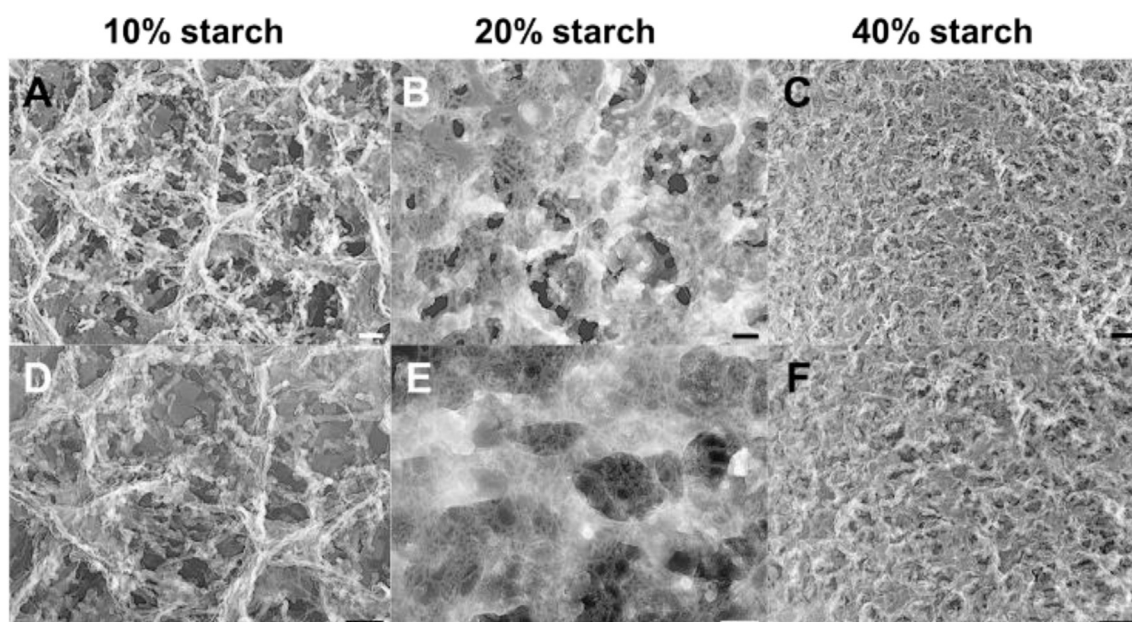
Fig. 2. TEM of replicas obtained from freeze-fractured, etched and replicated vitrified starch gel samples. Whereas 10% (w/v) starch gels show a comparatively wide-meshed secondary structure (A, D), 20% (w/v) starch gels contain a denser network of amylose and amylopectin double helices (B, E) leading to a more accurate differentiation between antibiotic permeabilities. Further increase of concentration (C, F) causes an even denser network but no improvement in differentiation. Pictures A–C: 68,000× magn., D–F: 98,000× magn. Colors were inverted. Scale bars represent 100 nm.

model optimization, clogD$_{pH7.4}$ and number of rotatable bonds were removed as input parameters to enhance robustness and avoid over-prediction. To ensure reproducibility, the seed value "6" was randomly selected.

The code used for the analysis is enclosed in the supplementary information. Physicochemical properties are available in Dataset S1.

Significance tests/Plots. Tests for significance and plotting of permeation data were carried out using GraphPad Prism® 7.04 software (GraphPad Prism software Inc., San Diego, CA, USA).

Results and discussion

Selection of polysaccharide gel

We selected the four polysaccharides: alginate, chitosan, slightly acid-degraded potato starch and agarose as gel-forming agents and coated 96-

well filters with these hydrogels using different concentrations and initially investigated the permeation of four representative antibiotics through those coatings. Out of these substances, ciprofloxacin (CIP) and tetracycline (TET) are reportedly high-accumulating compounds, which mainly follow porin-dependent uptake into the Gram-negative model bacterium *E. coli*. Rifampicin (RIF) and novobiocin (NOV) belong to low-accumulating compounds and are due to their larger size and lower hydrophilicity unlikely to have substantial porin-mediated uptake [8,17, 51–53]. Collecting time-resolved permeation data allowed for calculating apparent permeability coefficients (P$_{app}$) across the different coatings. This parameter being widely used for *in vitro* pharmacokinetic investigations represents the average permeation speed of a molecule and is a result of all possible transport phenomena (passive and active, uptake and efflux) during its passage through a membrane [39]. It commonly covers a wide range of measured permeation data, which leads to a more robust endpoint. Without any coating, permeation across the plain filter is rather fast and seems to favor reportedly
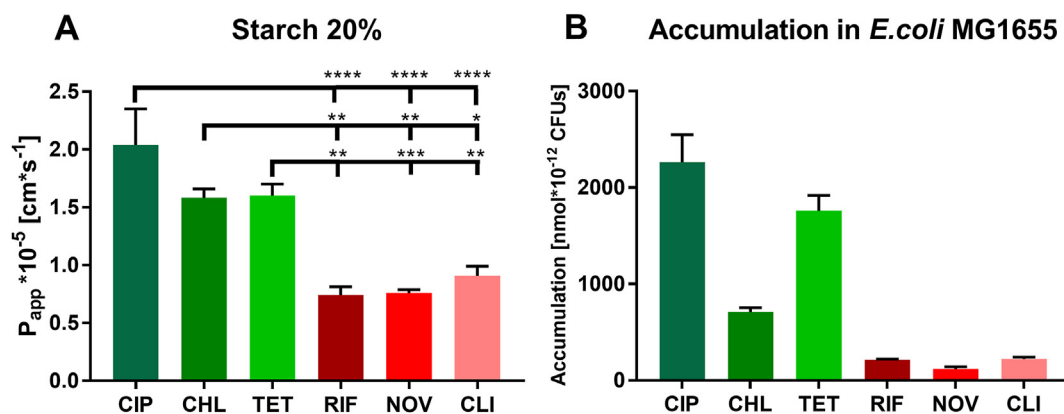

Fig. 3. Apparent permeability coefficients (P$_{app}$) of six antibiotics on a 20% starch gel membrane (A) in comparison to reported accumulation in *E. coli* MG1655 (B). P$_{app}$-values of high accumulating CIP, TET and CHL as well as low accumulating RIF, NOV and CLI are in qualitative agreement with *in bacterio* compound accumulation. Columns in (A) represent mean P$_{app}$ ± SEM, $n = 9$–11 from 3–4 independent experiments; a one-way ANOVA was performed with Tukey's post-hoc analysis. *$P < 0.05$, **$P < 0.01$, ***$P < 0.001$, ****$P < 0.0001$. Columns in (B) are mean accumulated amounts ± SEM, as reported [17].
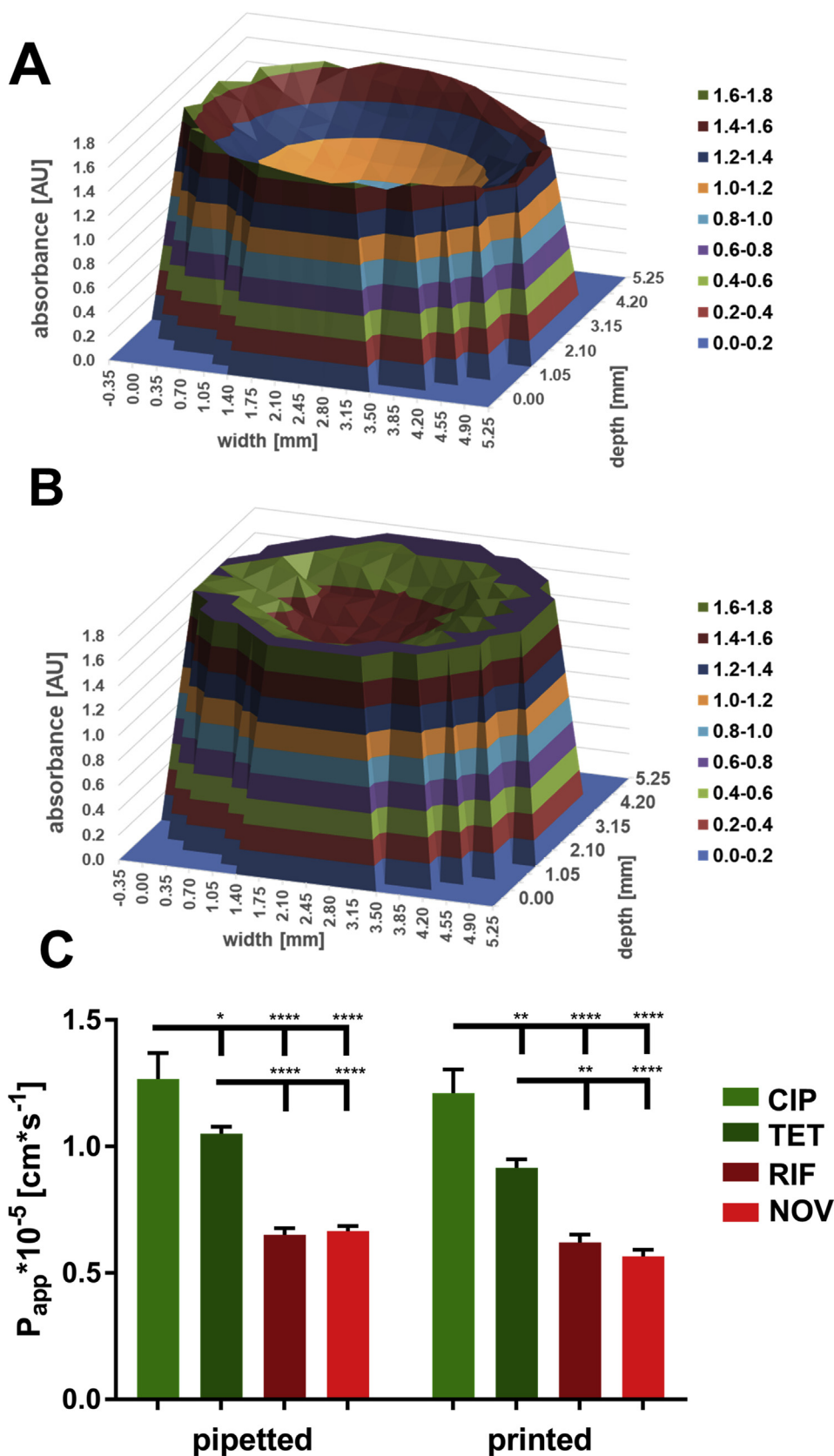
Fig. 4. Characterization and comparison of printed and pipetted membranes. Three-dimensional absorbance intensity plot of a representative pipetted (A) and printed (B) starch membrane. A higher and more homogenous absorbance distribution of the starch membrane accounts for an enhanced layer thickness and a less intense meniscus formation. Structural differences had minor impact on the permeation of CIP, TET, RIF and NOV (C). Columns represent mean $P_{app} \pm$ SD. A two-way ANOVA was performed with Tukey's post-hoc analysis. $n = 12$ from 3 independent experiments. *$P < 0.05$, **$P < 0.01$, ***$P < 0.001$, ****$P < 0.0001$.

low-accumulating NOV and RIF (Fig. S1). In contrast, permeation of the same compounds across the different gel coatings was largely in agreement with their known bacterial uptake. As we found, however, the 20% (w/v) starch gel performed best (Fig. S2 A) in distinguishing compounds

by their permeability, since it led to the most significant differences between the high and low accumulating compounds. Charge, as present in alginate and chitosan (Fig. S2 B, C), did not seem to play a crucial role. In the case of chitosan, the degree of deprotonation of the amine groups at

neutral pH was obviously still too low to affect permeability. Freeze-fracture images suggest that in comparison to the starch network, structures might be too wide (e.g., chitosan, Fig. S3 A–B) or too narrow (e.g., alginate, Fig. S3 C) to make a difference. Agarose as a further uncharged polymer forms a regularly meshed hydrogel network with larger pores (>100 nm, Fig. S3 D), obviously too large to discriminate the permeability of small antibiotic molecules. Additional permeability studies on the two starch components amylose and amylopectin (Fig. S2 E, F) demonstrate that discrimination between CIP and TET on the one hand and NOV and RIF on the other hand is more pronounced by the branched polysaccharide amylopectin, but still not as effective as a blend of both. The 20% (w/v) starch gel, according to our findings, leads to slightly denser polysaccharide networks of various and homogeneously distributed pore sizes (compare Fig. 2B,E to Fig. S3 E, F). Given that the number of polysaccharide meshes smaller than 100 nm is visibly high within the 20% starch gel, it is likely that novobiocin with a length of approx. 2 nm and a minimum projection area of 62 Å^2 undergoes stronger retention than ciprofloxacin with a length of approx. 1 nm and a minimum projection area of 43 Å^2. Considering that the mesh sizes and molecular sizes are highly varying, one must assume that the compound permeation is determined by two effects: hydrodynamic effects, when permeating through larger meshes, and obstructive effects, when permeating through or along small meshes in the polymer network [54, 55]. Especially in the latter case, the negative charge of NOV and zwitterionic state of CIP at pH 7.4, as well as the dipole moment (10 vs. 43 Debye) may play an additional role because of the close proximity to hydroxyl groups of the glucose units in the starch gel network. Lower starch concentrations as well as higher concentrations may again lead to suboptimal network densities (Fig. 2A,D and C,F)..

The additional investigation of the high-accumulating chloramphenicol (CHL) and the low-accumulating clindamycin (CLI) on the 20% starch formulation also leads to an accurate separation by their P_{app} (Fig. 3). This is noteworthy considering that CLI and TET are of similar molecular mass (444.44 Da vs. 424.98 Da, respectively). Moreover, it indicates that additional factors other than solely molecular size must be considered to explain their different permeability coefficients.

Printing of polysaccharide gel on filter membranes

Hydrogels undergo continuous changes from the time of formation until the time of use. These changes include aggregation, syneresis, phase changes, crystallization and retrogradation [56–58]. Thus, it is recommended to treat hydrogels strictly according to the established protocol to obtain comparable results. Temperatures should be kept constantly above the gelation temperature during the coating and storage temperatures as well as storage duration should remain constant. Automating the production process may support the uniform handling of hydrogels and is a reasonable measure for larger throughput efforts. Therefore, before investigating a larger set of antibiotics with such set up, we automated the membrane preparation using a customized modular and multifunctional printer (Fig. S4). This printer features a heated Hamilton® syringe as a print head, allowing to extrude and distribute equal amounts of 40 μL starch solution into each well before gel formation.

Topological characteristics of the starch coatings were investigated by scanning their absorbance in a plate reader at 666 nm after staining with methylene blue. For each well, 177 different locations were measured in a filled circle pattern. In our studies, printed membranes generally had a higher average absorbance per well than manually pipetted membranes (Fig. 4 A, B; Fig. S5 A), indicating an increased thickness. Moreover, the starch distribution of printed coatings was more homogenous, both within and between the produced batches (Figs. S5B-D, S6A,B). In addition, the formation of a meniscus was less prominent after printing (Fig. 4A,B). In order to evaluate the accuracy of the printed membrane model, we studied the permeability of the previously employed panel of CIP, TET, RIF and NOV on printed starch membranes and compared the results to those manually prepared (Fig. 4C, Fig. S7). While the

permeability pattern of the four selected antibiotics was essentially the same, permeation of tetracycline through the printed starch membrane was decreased, reflecting that printed coatings were slightly thicker than pipetted ones.

The standard deviation of the obtained permeability coefficients did not noticeably change, when the starch gel was printed, suggesting that the main causes of errors do not happen during the coating process.
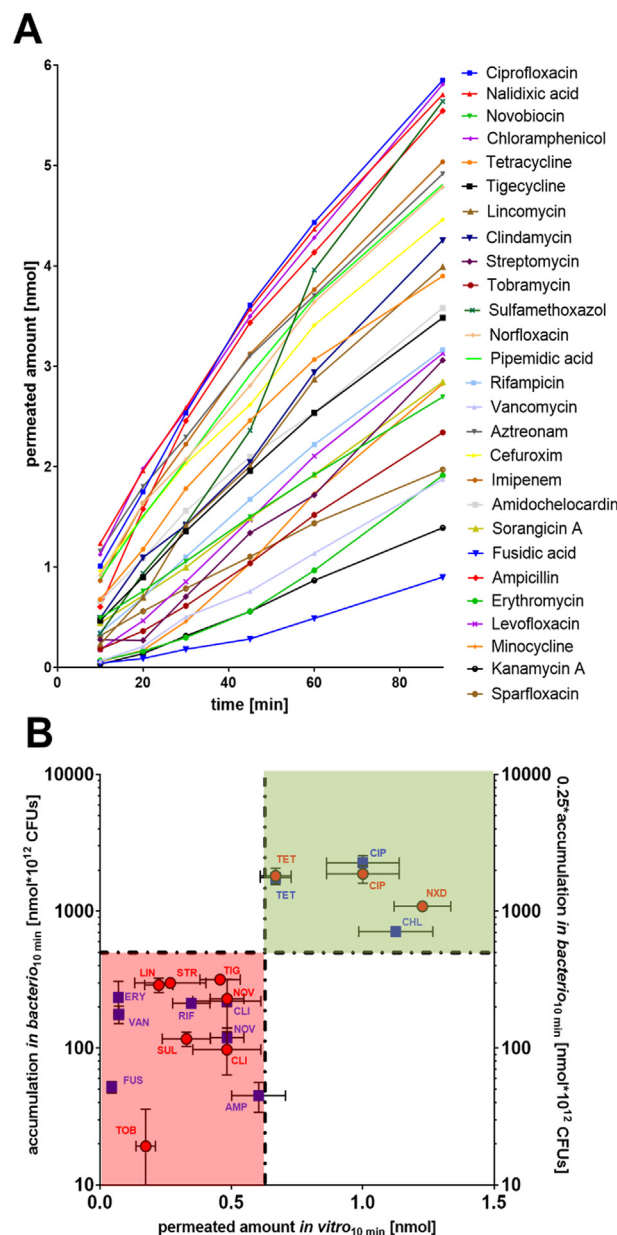

Fig. 5. Antibiotic permeation *in vitro* compared to *in bacterio* accumulation. A) Permeation-time course of 27 antibiotics across the starch based *in vitro* model, showing their different permeation kinetics (Error bars not shown; full dataset in Table S4). B) Quadrant plot of obtained permeated amounts from the *in vitro* starch model and their accumulation *in bacterio*. The *in bacterio* as well as the *in vitro* data show a separation into high (green quadrant) and low accumulating (red quadrant) antibiotics. To correct for a four times higher initial drug concentration used for the self-generated data (red circles), the accumulated amounts were multiplied by 0.25. Blue squares depict reported *in bacterio* accumulation [17]. Points represent mean permeated amounts ± SEM, $n_{in\ vitro}$ = 11–16 from 3–4 independent experiments. $n_{in\ bacterio}$ = 4 from 2 biological replicates.
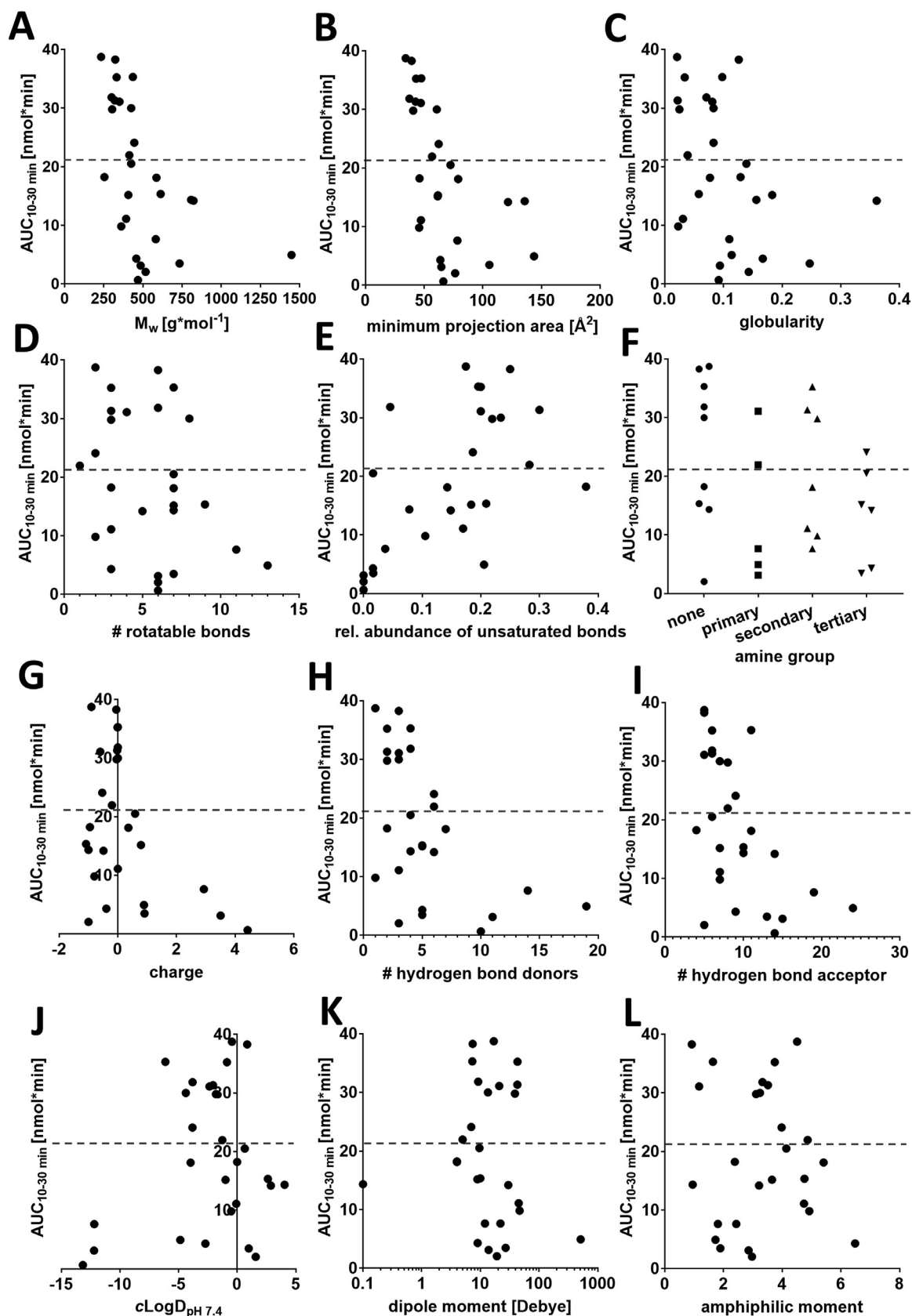
Fig. 6. Correlations between drug permeation and selected physicochemical parameters. From 27 antibiotics, the $AUC_{10–30\ min}$ as representative parameter for permeation is plotted against (A) molecular mass, (B) minimum projection area, (C) globularity, (D) number of hydrogen bond donors and (E) acceptors, (F) net charge, (G) type of amine group, (H) number of rotatable bonds, (I) relative abundance of unsaturated bonds, (J) $c$log$D_{pH7.4}$ (K) dipole moment and (L) amphiphilic moment (vsurf_A). The dashed line represents the set $AUC_{10–30min}$ threshold of 21 nmol × min.
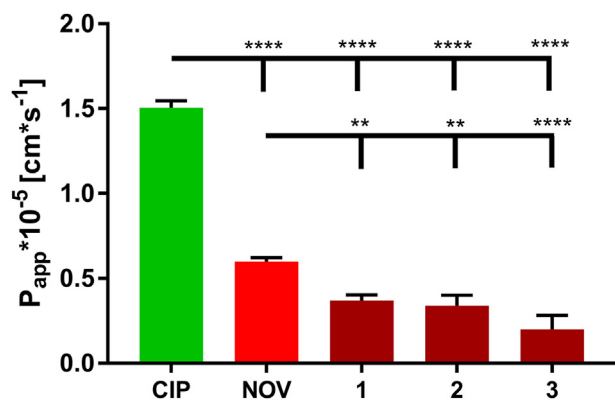
Fig. 7. Assessment of the permeability of RNA polymerase inhibitors 1–3. The comparison to high accumulating CIP and low accumulating NOV indicates that all presented RNAP-inhibitors likely belong to low accumulating drugs, whereas **3** probably accumulates particularly low. Columns represent mean P_{app} ± SEM; $n = 9$–12 from three independent experiments. One-way ANOVA was performed with Tukey's post-hoc analysis. ****$P < 0.0001$, **$P < 0.01$.

Validation of the assay

After automation of the membrane-coating process, we selected 27 antibiotics and generated *in vitro* membrane-permeability data to validate the model (Fig. 5A, Table S4). Among those, the *in vitro* permeability of 16 compounds was compared to their *in bacterio* accumulation in *E. coli* K-12 strain MG1655 using the 10 min time point, obtained not only from literature [17], but also from own experiments (Fig. 5 B).

Notably, all compounds could be consistently divided into a high-accumulating (green area) and a low-accumulating group (red area), which surpassed the initial expectation considering the comparison of passive permeation across a hydrogel with accumulation inside a fully functional bacterium being also able to actively pump out antibiotics. TET, CIP, CLI and NOV served to demonstrate the comparability of own and reported *in bacterio* data. A clear separation between high-accumulating CIP and TET and low-accumulating NOV and CLI, respectively, is noticeable and confirms a comparable outcome.

By looking more specifically at the gyrase inhibitors nalidixic acid (NAL) and CIP, both reach a high permeability *in vitro* as well as a high level of accumulation *in bacterio*, even though NAL accumulates more slowly, as can also be seen in the accumulation time course (Fig. S8). Previous studies on a multiple lipid-layered membrane model as well as *E. coli* mutants indicated that in contrast to CIP, NAL has a substantial porin-independent uptake into *E. coli* [42,59]. This could be also confirmed by studies on an *in vitro* outer membrane model being composed of LPS and phospholipids only (Fig. S9), where NAL and NOV permeate faster than reportedly porin-dependent CIP and CHL [6,11]. Comparing this outcome to the permeability data from the starch model confirms that the latter model mainly mimics porin-mediated permeation, since it allows for good permeation of CIP and TET compared to

Table 1
Most influential physicochemical parameters according to random forest analysis.

Feature	%IncMSE
Molecular mass	33.86
Minimum projection area	32.82
Relative abundance of unsaturated bonds (rigidity)	16.00
Number of hydrogen bond acceptors	4.42
Number of hydrogen bond donors	3.74
Net charge	3.56
Amphiphilic moment (vsurf_A)	3.14
Globularity	2.73
Dipole moment	1.63

NOV. Interestingly, however, NAL permeates fast across the starch model as well as the OM model, while it also has a high accumulation *in bacterio*. It is worth mentioning that attributing its good accumulation to high porin permeability seems implausible, considering reports on its good permeability across LPS and membrane phospholipids. The outstandingly high permeability of NAL through our starch model gives evidence that this model may to some extent also mimic porin-independent passive permeation.

Regarding the tetracyclines, tigecycline (TIG) shows a slow but steadily increasing accumulation and permeation compared to TET (Fig. S8). Its 9-*t*-(butylglycylamido) moiety, seems to sterically delimit the access via the unspecific bacterial porins OmpC and OmpF [60] and also impede the permeation through the starch network *in vitro*. Additionally, TIG is known for its decreased efflux, mediated by its side chain [61], which explains its steadily increasing accumulated amount over time without fluctuation *in bacterio*. Another class that turned out to be low accumulating is the aminoglycosides. In agreement to their low accumulation, low permeation of tobramycin (TOB) and streptomycin (STR) can be observed in our *in vitro* model, which is probably due to hydrogen bond formation with the hydroxyl-groups of the glucose units of starch. The same effect may occur with LPS, while aminoglycosides permeate across the outer membrane in course of "self-promoted uptake" [11]. Clindamycin and lincomycin, which both feature a carbohydrate structure, may suffer from the same mechanism of retention like aminoglycosides. Notably, we observed low accumulation of sulfamethoxazole (SUL) in *E. coli* despite its low molecular size. Since its entry route is so far largely unknown, one can only speculate that it is perhaps the absence of a positive charge or a zwitterionic structure that delimits its permeation across OmpC and OmpF or an increased efflux. Comparing the accumulation-time course *in bacterio* to the permeation-time course *in vitro*, reveals the highest accuracy of the *in vitro* model within the early time interval of 10–30 min (Fig. 5A, Fig. S8). Obviously, in absence of any active-transport mechanisms, this assay may, however, not provide valid data for antibiotics that undergo TonB-dependent transport, such as cefiderocol and other future siderophore antibiotics. Peptides with membrane-disruptive or pore-forming effects, such as colistin, polymyxin B and daptomycin, are unsuitable test components for this model, since their mechanism of action is strongly dependent on the presence of membrane phospholipids. As their target is the bacterial membrane itself, the investigation of their translocation is not required.
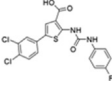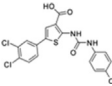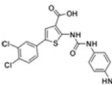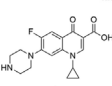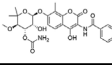
Structure–permeability relationships

Since a nonlinear phase of permeation behavior occurred for some compounds, the area under the curve ($AUC_{10–30\ min}$) was calculated (Dataset S1) and used instead of P_{app} for investigations regarding structure–permeability relationships. Besides, a threshold value was introduced classifying substances with an $AUC_{10–30min} < 21$ nmol × min as low permeating, whereas all other molecules were regarded as high-accumulating (Table S5). This threshold leads to the most accurate classification of all previously discussed compounds.

On this basis, we investigated structure–permeability relationships from our *in vitro* model and compared the outcome to currently discussed factors that determine compound accumulation in Gram-negative bacteria [6,36,37,62,63].

In line with previous findings *in bacterio* [35,36], molecular mass (M_w) also determines the permeability of compounds through the gel model. A decrease in permeation can be observed, when plotting the molecular mass of our panel of antibiotics against their $AUC_{10–30\ min}$ (Fig. 6A) with an apparent cut-off at *ca.* 500 Da. This value seems lower than the widely assumed permeation cut-off of *ca.* 600 Da [8,64,65]. *Accumulation*, however, is—apart from uptake—also a function of efflux. Studies by Brown et al. indicate that especially those compounds with Mw between 450 Da and 600 Da undergo efflux in *E. coli* and *Pseudomonas aeruginosa* [37]. This peculiarity might have contributed to the good match between *in vitro* permeation and *in bacterio* accumulation.

Table 2
Antibacterial and physicochemical properties of RNA polymerase inhibitors, CIP and NOV.

ID	Structure	Activity			Permeability	Molecular descriptors								
		IC$_{50}$ [µM][a]	MIC$_{95}$ [µM][b]	MIC$_{95}$ [µM][c]	P$_{app}$ × 10^{-5} [cm*s^{-1}] ± SEM	Min. proj. area [A^2]	Mw [Da]	Rigidity	Net charge (pH 7.4)	# HBA	# HBD	Glob.	Amphiphilic moment	Dipole moment [Debye]
1		14	4	33	0.37 ± 0.03	55.59	425.3	0.43	−1.00	3	3	0.011	4.906	10
2		22	8	23	0.34 ± 0.06	66.38	437.3	0.45	−1.00	4	3	0.013	4.269	13
3		8	3	>50	0.20 ± 0.08	88.97	562.4	0.48	−1.24	5	4	0.050	3.680	18
C I P		3.9	>2[d]	0.13	1.51 ± 0.04	43.14	331.3	0.20	−0.01	6	2	0.034	3.748	43
NOV		0.5	>2[e]	2.6	0.60 ± 0.02	61.67	612.6	0.21	−1.08	10	5	0.058	4.758	10

[a] Half inhibitory concentrations for *E. coli* RNA polymerase (**1–3**) [48] and *E. coli* DNA gyrase (CIP and NOV) [69].
[b] MIC values against *S. aureus* Newman, (**1–3**) [48].
[c] MIC values against *E. coli* ΔTolC (efflux-deficient).
[d] Growth inhibition at 2 µM: 83% ± 12.
[e] Growth inhibition at 2 µM: 87% ± 5.

Another distinct dependency was found between minimum projection area and drug permeation (Fig. 6 B). This value being a hybrid parameter for molecular mass and three-dimensionality may be particularly helpful in drug development, since it implies that a potentially low accumulation due to high molecular mass can be compensated by reducing the spatial molecular expansion.

Similar conclusions were drawn already recently [63]. By looking at the dependency between permeation and globularity a correlation can also be observed, even though it is less strong, if compared to the previous parameters (Fig. 6C).

As for rigidity, unlike previously reported [17], no clear correlation could be found between AUC$_{10-30\ min}$ and number of rotatable bonds (Fig. 6D). However, it seems plausible to use rather a relative parameter that is normalized to molecular size. By considering the relative number of unsaturated bonds instead, we could indeed demonstrate a direct correlation between molecular rigidity and AUC$_{10-30\ min}$ (Fig. 6E). In contrast, no clear tendency was found among compounds with amine groups: only 2 compounds with a primary amine showed high accumulation, whereas 9 of the high-accumulating drugs did not feature any primary amine. Moreover, 7 compounds with a general amine (primary, secondary or tertiary) highly accumulated, whereas 12 compounds featuring an amine accumulated low (Fig. 6F).

Rather impressively for a noncharged membrane, molecular net charge appears to affect permeation. A permeation optimum was reached at a net charge close to zero (Fig. 6G). This phenomenon may be attributed to ion–dipole interactions of permeating molecules to the hydroxyl groups of the polysaccharide network. In this regard, it is important to mention that most of the well-permeating drugs *in vitro* are zwitterions at pH 7.4 (8 out of 11), whereas the majority of low-accumulating antibiotics is not (3 out of 14). The preferred permeation of zwitterionic compounds was also reported for the porin OmpF [19], where, however, ion-ion interactions determine the translocation [25].

In line with earlier studies [36], we observed that the number of hydrogen bond donors and acceptors had impact on antibiotic permeation *in vitro* (Fig. 6 H,I). In both cases, a low number was associated to better permeation. Notably, clogD$_{pH7.4}$ as parameter for hydrophilicity or lipophilicity, also seemed to influence drug permeation, since molecules with clogD$_{pH7.4}$ values between 0 and –5 permeated best (Fig. 6J). This is in agreement with previous assumptions about an enhanced permeation of slightly hydrophilic compounds as a typical feature of porin-mediated uptake [6,27,36].

Moreover, the dipole moment [32,66] and amphiphilic moment [67] are discussed to have influence on compound permeability. However, plots of the respective parameters against AUC$_{10-30\ min}$ do not reveal obvious correlations.

Since a plot-based discussion of the impact of the aforementioned physicochemical properties is rather biased, we employed a random-forest (RF) regression model to more objectively investigate and rank these properties according to their impact on *in vitro* permeability. Our RF was generally trained with 26 out of 27 tested compounds, whereas the AUC$_{10-30\ min}$ of the 27th compound was predicted to be high- or low-accumulating. This was done in 27 cycles, each time predicting the AUC$_{10-30\ min}$ of another 27th compound after training the model with the remaining 26 substances. To assess the impact of the physicochemical parameters on the prediction, we systematically left one parameter out of the RF and compared the increase of prediction error (%lncMSE). In this way, the first RF regression confirmed nine factors (molecular mass, minimum projection area, rigidity, number of hydrogen bond donors and acceptors, globularity, charge, amphiphilic moment and dipole moment) to be critical. For the remaining parameters, the RF was repeated. With this run, we obtained a ranking of the parameters according to their importance for the prediction (Table 1).

The RF confirmed the previously discussed parameters molecular mass, minimum projection area, relative abundance of unsaturated bonds, hydrogen bond donors as well as acceptors, net charge, amphiphilic moment, globularity and dipole moment as major parameters governing the permeation across this starch model. Nevertheless, the low impact or absence of parameters, such as clogD, rotatable bonds and dipole moment and the high impact of molecular weight suggest that this model does not only mimic porin-mediated permeation. This balanced selectivity, being a result of combined hydrodynamic and obstructive diffusion phenomena inside the starch gel network, obviously allows for both: the discrimination between high and low accumulating small molecules that would either follow the porin-dependent or the porin-

independent passive pathway.

When applying the previously mentioned threshold of 21 nmol × min on the predicted AUC$_{10-30 \text{ min}}$, we achieved an accuracy of around 81% compared either to AUC$_{10-30 \text{ min}}$ obtained by our *in vitro* assay or to *in bacterio* compound accumulation (Table S5).

Application

Having demonstrated associations between *in vitro* permeation and *in bacterio* accumulation, we applied our assay to in-house small-molecule RNA polymerase inhibitors **1**–**3** with high activity against Gram-positive *S. aureus* [48] but inactivity against Gram-negative *E. coli* wildtype [49] and limited activity against the efflux-deficient *E. coli* ΔTolC strain (Table 2).

While antibacterial activities (MIC$_{95}$) against *S. aureus* correlate with the target inhibition (IC$_{50}$), this is not the case for *E. coli* ΔTolC. This suggests that the activity against *E. coli* might be delimited because of low compound uptake, possibly because of their negative charge. Especially, the uptake of compound **3** seems limited considering the high MIC$_{95}$ despite its rather potent target inhibition (IC$_{50}$ = 8 μM).

Surprisingly, in our starch gel–based *in vitro* study P$_{app}$-values of all

three RNAP inhibitors were indeed significantly lower than those of NOV, clearly classifying them as compounds with low permeability and with compound **3** permeating particularly poorly (Fig. 7).

Generally, permeability data from the starch-based model in comparison to activity data of **1**–**3** as well as CIP and NOV are in better agreement for *E. coli* than for the Gram-positive *S. aureus*, which corroborates the notion that this model is relevant only for Gram-negative bacteria.

While all our readouts were obtained by directly measuring absorbance in a plate reader, the model may also be expanded to contemporary LC–MS methods [68].

Predicting activity in different bacterial strains

Finally, we wanted to explore direct associations between *in vitro* permeability and antibacterial activity against Gram-negative and Gram-positive bacterial species mentioned in the priority list by the World Health Organization [70]. For this purpose, we compared the most abundantly reported MIC values from the European Committee for Antimicrobial Susceptibility Testing (EUCAST) database for *E. coli*, *P. aeruginosa*, *Acinetobacter baumannii*, *Klebsiella pneumoniae*, *Campylobacter jejuni*, *Salmonella* spp., *Neisseria gonorrhoeae*, *Staphylococcus aureus*
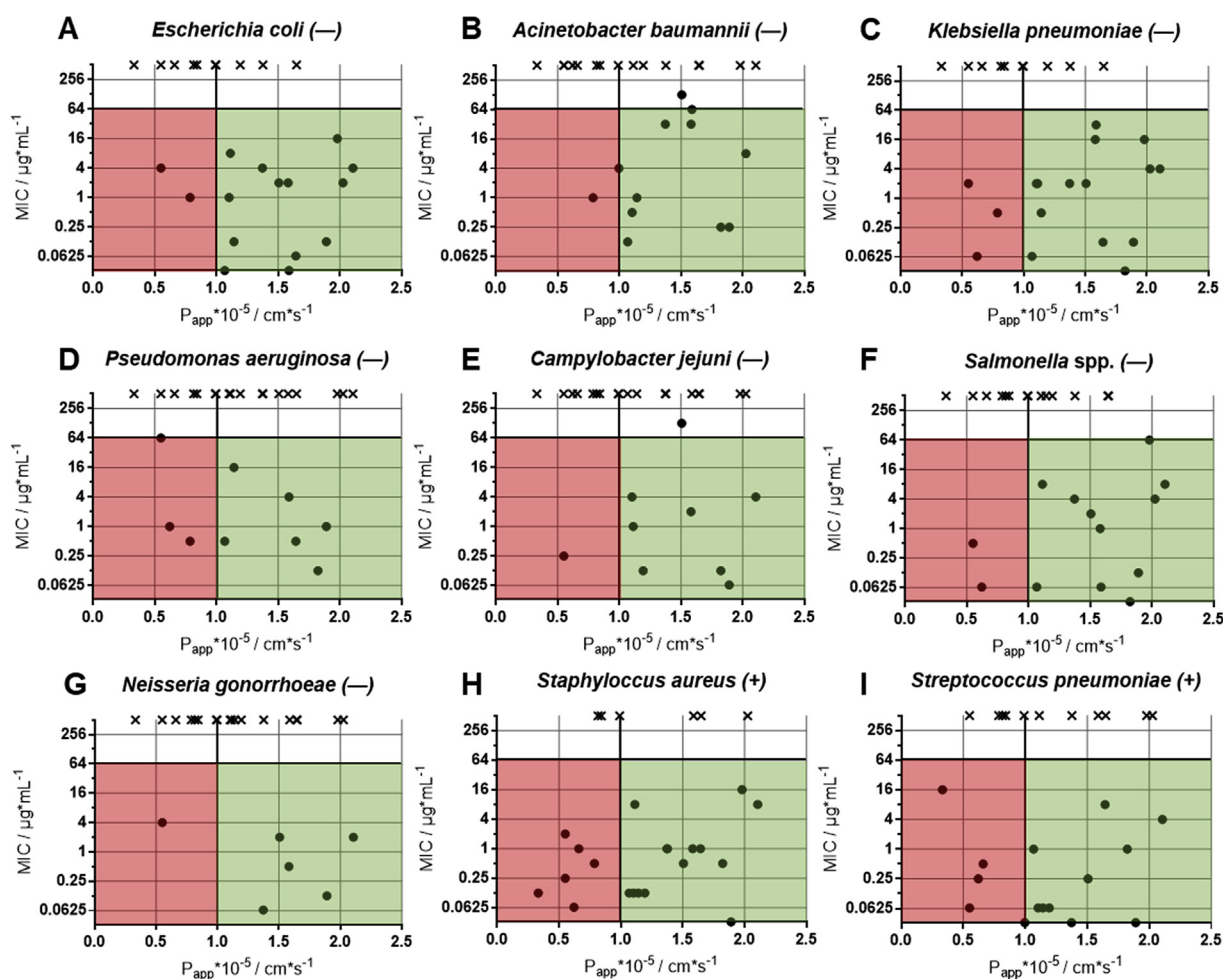

Fig. 8. Quadrant plot of *in vitro* permeability and *in bacterio* activity relationships for *Escherichia coli* (A), *Acinetobacter baumannii* (B), *Klebsiella pneumoniae* (C), *Pseudomonas aeruginosa* (D), *Campylobacter jejuni* (E), *Salmonella* spp. (F) and *Neisseria gonorrhoeae* (G), *Staphylococcus aureus* (H) and *Streptococcus* pneumoniae (I). Arbitrarily set lines at an apparent permeability coefficient (P$_{app}$) of 1 × 10^{-5} cm/s and a minimum inhibitory concentration (MIC) of 64 μg/mL demonstrate that, for the majority of all 27 candidate antibiotics tested, low MIC values are associated with high permeability (green quadrant). *Vice versa*, for the Gram-negative species (−) low *in vitro* permeability is associated with poor antibacterial activity. Only few points show activity in spite of low *in vitro* permeability (red quadrant = false negatives). In contrast, good activity against Gram-positive species (+) was frequently found among substances with poor *in vitro* P$_{app}$. Crosses indicate non-available MICs according to EUCAST standards and were arbitrarily set to >256 μg/mL.

and *Streptococcus pneumoniae* [71] with the P_{app}-values for 27 compounds as measured by the starch hydrogel assay (Fig. 8, Dataset S1).

Obviously, throughout all seven Gram-negative species, antibacterial activity of a given compound is—with very few exceptions—associated with a P_{app} above 10^{-5} cm/s. For antibiotics with intracellular targets, permeability across the Gram-negative bacterial cell envelope represents a necessary but not sufficient condition for antibacterial activity. Measuring the P_{app}-value *in vitro* allows identifying compounds, which are unlikely to achieve sufficient concentrations to be active *in bacterio*. Compounds with antibiotic activity despite low permeability would therefore represent false negatives of such assay. However, those were only 1–3 of 27 compounds among the seven Gram-negative strains, while four or six false negative cases were found for the Gram-positive strains *S. pneumoniae* or *S. aureus*, respectively. This simple *in vitro* assay therefore opens the perspective not only to predict *in bacterio* accumulation but also to exclude probably inactive antibiotics at an early stage of drug development with focus on Gram-negative bacteria. For Gram-positive bacteria, however, this assay seems less suitable.

Conclusion

We investigated different polysaccharide hydrogels with the aim to find functional properties that allow for the prediction of antibiotic accumulation in Gram-negative bacteria. Freeze-fracture TEM of gel-networks from different polysaccharides and concentrations revealed a remarkable diversity of network structures and porosity. A 20% (w/v) starch hydrogel model proved highly competent to discriminate high from low-accumulating antibiotics in the Gram-negative model bacterium *E. coli*. The fast permeation of porin-dependent antibiotics, as has been found in the starch gel, shows that this model mainly mimics the Gram-negative specific porin-mediated uptake. However, permeation data of nalidixic acid and structure-permeability relationships suggest that this model also identifies high-accumulating compounds with good porin-independent permeation across the outer membrane.

The preparation of the model, regardless if manually pipetted or printed, is simple, reproducible, cost-effective and hazard-free. While uptake studies in living bacteria or artificial vesicles are cumbersome to perform, membrane-permeation experiments can be automated and deliver accurate results within 10 min, making it compatible with high-throughput screening applications on molecules with various physico-chemical properties.

Applying contemporary tools of machine learning to our *in vitro* data provided evidence to the impact of molecular characteristics, which were reported earlier *in bacterio*. Although due to obvious differences between the chosen polysaccharide and the bacterial cell envelope, we found that a small set of seven features was sufficient of create a robust machine learning model with good prediction based on *in vitro* permeation data. In the context of studying *in vitro* permeability of structurally diverse antibiotics, we also report the first data on *in bacterio* accumulation of aminoglycosides and sulfonamides—important classes of antibiotics to treat Gram-negative infections.

By applying the gel-based assay on in-house synthesized antibiotics, we could find an explanation for their low activity against Gram-negative bacteria. Expanding the investigations to antibiotic activity against highly relevant Gram-negative species gave evidence that *in vitro* permeability data may allow to exclude inactive substances at an early stage of antibiotic development.

Room for further improvements of the model may consist in the use of starches with different ratios of amylose and amylopectin, as well as further variation of gel concentrations and charges to obtain a more pathogen-specific prediction. The addition of β-lactamases or penicillin binding proteins to the acceptor compartment may lead to enhanced accuracy regarding β-lactam antibiotics. Prospectively, by refining the composition of the alginate formulation or the application of biological hydrogels, the described assay can be modified towards investigating permeability across biofilms, exopolysaccharides or mucus on larger scale.

Author Contributions

Robert Richter: Methodology[1], Validation[1], Formal analysis[1], Conceptualization[1], Investigation[1], Data Curation[1], Writing – Original Draft, Software (g-code), Visualization.

Mohamed A. M. Kamal: Investigation[1], Formal analysis[1], Writing – Review & Editing

Mariel Garcia-Rivera: Methodology[2], Investigation[2], Formal analysis[2]

Mark Brönstrup: Supervision[2], Funding Acquisition[2], Resources[2], Writing – Review & Editing

Walid A. M. Elgaher: Investigation[3], Writing – Review & Editing

Rolf W. Hartmann: Supervision[3], Resources[3], Funding Acquisition[3], Project administration[3]

Anna K. H. Hirsch: Supervision[3], Resources[3], Funding Acquisition[3], project administration[3], Writing – Review & Editing

Maximilian Junk: Software[4], Methodology[4], Investigation[4].

Jerome Kaspar: Conceptualization[4], Supervision[4] Writing – Review & Editing

Michael Vielhaber: Supervision[4], Resources[4]

Sanjay K. Srikakulam: Software (R-code)[5], Formal Analysis[5].

Alexander Gress: Formal Analysis[5]

Olga Kalinina: Supervision[5], Writing – Review & Editing

Alexander Grißmer: Investigation[6]

Anja Beckmann: Investigation[6], Methodology[6], Writing – Review & Editing

Carola Meier: Supervision[6], Methodology[6]

Nicole Schneider-Daum: Supervision[1], Writing – Review & Editing

Claus-Michael Lehr: Funding acquisition[1], Project administration[1], Supervision[1], conceptualization[1], Writing – Review & Editing

Declaration of competing interest

The authors declare that they have no known competing financial interests or personal relationships that could have appeared to influence the work reported in this paper.

Acknowledgements

---

[1] regarding the *in vitro* model or obtained data, respectively.

[2] regarding the bacterial control assay.

[3] regarding the design, synthesis, and biological evaluation of RNAP inhibitors.

[4] regarding the construction of the printer.

[5] regarding the random forest analysis.

[6] regarding the freeze fracture TEM.

Appendix A. Supplementary data

Supplementary data to this article can be found online at https://doi.org/10.1016/j.mtbio.2020.100084.

References

[1] C. Nathan, O. Cars, Antibiotic resistance - problems, progress, and prospects, N. Engl. J. Med. 371 (2014) 1761–1763, https://doi.org/10.1056/NEJMp1408040.

[2] L.L. Silver, Challenges of antibacterial discovery, Clin. Microbiol. Rev. 24 (2011) 71–109, https://doi.org/10.1128/CMR.00030-10.

[3] B. Aslam, W. Wang, M.I. Arshad, M. Khurshid, S. Muzammil, M.H. Rasool, M.A. Nisar, R.F. Alvi, M.A. Aslam, M.U. Qamar, M.K.F. Salamat, Z. Baloch, Antibiotic resistance: a rundown of a global crisis, Infect. Drug Resist. 11 (2018) 1645–1658, https://doi.org/10.2147/IDR.S173867.

[4] U. Theuretzbacher, S. Gottwalt, P. Beyer, Antibacterial Agents, WHO, 2017, https://doi.org/10.1007/978-3-662-44000-1_14, 0–48.

[5] E.D. Brown, G.D. Wright, Antibacterial drug discovery in the resistance era, Nature 529 (2016) 336–343, https://doi.org/10.1038/nature17042.

[6] H. Nikaido, Molecular basis of bacterial outer membrane permeability revisited, Microbiol. Mol. Biol. Rev. 67 (2003) 593–656, https://doi.org/10.1128/MMBR.67.4.593.

[7] R.E.W. Hancock, Role of porins in outer membrane permeability, J. Bacteriol. 169 (1987) 929–933, https://doi.org/10.1128/jb.169.3.929-933.1987.

[8] R.S. Santos, C. Figueiredo, N.F. Azevedo, K. Braeckmans, S.C. De Smedt, Nanomaterials and molecular transporters to overcome the bacterial envelope barrier: towards advanced delivery of antibiotics, Adv. Drug Deliv. Rev. 136–137 (2018) 28–48, https://doi.org/10.1016/j.addr.2017.12.010.

[9] J.W. Costerton, K.-J. Cheng, The role of the bacterial cell envelope in antibiotic resistance, J. Antimicrob. Chemother. 1 (1975) 363–377, https://doi.org/10.1093/jac/1.4.363.

[10] F. Graef, S. Gordon, C.M. Lehr, Anti-infectives in drug delivery—overcoming the gram-negative bacterial cell envelope, Curr. Top. Microbiol. Immunol. 398 (2016) 475–496, https://doi.org/10.1007/82.

[11] R.E.W. Hancock, A. Bell, Antibiotic uptake into gram-negative bacteria, Eur. J. Clin. Microbiol. Infect. Dis. 7 (1988) 713–720, https://doi.org/10.1007/BF01975036.

[12] T. Nakae, Outer-membrane permeability of bacteria, Crit. Rev. Microbiol. 13 (1986) 1–62, https://doi.org/10.3109/10408418609108734.

[13] J.M. Pagès, C.E. James, M. Winterhalter, The porin and the permeating antibiotic: a selective diffusion barrier in Gram-negative bacteria, Nat. Rev. Microbiol. 6 (2008) 893–903, https://doi.org/10.1038/nrmicro1994.

[14] M. Masi, M. Réfregiers, K.M. Pos, J.M. Pagès, Mechanisms of envelope permeability and antibiotic influx and efflux in Gram-negative bacteria, Nat. Microbiol. 2 (2017), https://doi.org/10.1038/nmicrobiol.2017.1.

[15] J. Vergalli, A. Atzori, J. Pajovic, E. Dumont, G. Malloci, M. Masi, A.V. Vargiu, M. Winterhalter, M. Réfrégiers, P. Ruggerone, J.M. Pagès, The challenge of intracellular antibiotic accumulation, a function of fluoroquinolone influx versus bacterial efflux, Commun. Biol. 3 (2020) 1–12, https://doi.org/10.1038/s42003-020-0929-x.

[16] S. Acosta-Gutiérrez, I. Bodrenko, M. Ceccarelli, Permeability through Bacterial Porins Dictates Whole Cell Compound Accumulation, ChemRxiv, 2020, https://doi.org/10.26434/chemrxiv.11877834.v1 Preprint.

[17] M.F. Richter, B.S. Drown, A.P. Riley, A. Garcia, T. Shirai, R.L. Svec, P.J. Hergenrother, Predictive compound accumulation rules yield a broad-spectrum antibiotic, Nature 545 (2017) 299–304, https://doi.org/10.1038/nature22308.

[18] J.A. Bafna, E. Sans-Serramitjana, S. Acosta-Gutiérrez, I.V. Bodrenko, D. Hörömpöli, A. Berscheid, H. Brötz-Oesterhelt, M. Winterhalter, R. Ceccarelli, Kanamycin uptake into Escherichia coli is facilitated by OmpF and OmpC porin channels located in the outer membrane, ACS Infect. Dis. 6 (7) (2020) 1855–1865, https://doi.org/10.1021/acsinfecdis.0c00102.

[19] F. Yoshimura, H. Nikaido, Diffusion of β-lactam antibiotics through the porin channels of Escherichia coli K-12, Antimicrob. Agents Chemother 27 (1985) 84–92, https://doi.org/10.1128/AAC.27.1.84.

[20] S. Galdiero, A. Falanga, M. Cantisani, R. Tarallo, M. Elena Della Pepa, V. D'Oriano, M. Galdiero, Microbe-host interactions: structure and role of gram-negative bacterial porins, Curr. Protein Pept. Sci. 13 (2013) 843–854, https://doi.org/10.2174/13892031280487120.

[21] H. Nikaido, E.Y. Rosenberg, Porin channels in Escherichia coli: studies with liposomes reconstituted from purified proteins, J. Bacteriol. 153 (1983) 241–252.

[22] R.J. Ferreira, P. Kasson, Antibiotic uptake across gram-negative outer membranes: better predictions towards better antibiotics, ACS Infect. Dis. 5 (12) (2019) 2096–2104, https://doi.org/10.1021/acsinfecdis.9b00201.

[23] T. Nakae, Outer membrane of Salmonella typhimurium: reconstitution of sucrose-permeable membrane vesicles, Biochem. Biophys. Res. Commun. 64 (1975) 1224–1230.

[24] E.M. Nestorovich, C. Danelon, M. Winterhalter, S.M. Bezrukov, Designed to penetrate: time-resolved interaction of single antibiotic molecules with bacterial pores, Proc. Natl. Acad. Sci. U.S.A. 99 (2002) 9789–9794, https://doi.org/10.1073/pnas.152206799.

[25] H. Bajaj, S. Acosta Gutierrez, I. Bodrenko, G. Malloci, M.A. Scorciapino, M. Winterhalter, M. Ceccarelli, Bacterial outer membrane porins as electrostatic nanosieves: exploring transport rules of small polar molecules, ACS Nano 11 (2017) 5465–5473, https://doi.org/10.1021/acsnano.6b08613.

[26] J. Wang, R. Terrasse, J.A. Bafna, L. Benier, M. Winterhalter, Electrophysiological characterization of transport across outer membrane channels from Gram-negative bacteria in presence of lipopolysaccharides (LPS), Angew. Chem. Int. Ed. (2020) 1–6, https://doi.org/10.1002/anie.201913618.

[27] W. Zimmermann, A. Rosselet, Function of the outer membrane of Escherichia coli as a permeability barrier to beta lactam antibiotics, Antimicrob. Agents Chemother. 12 (1977) 368–372, https://doi.org/10.1128/AAC.12.3.368.

[28] G. Decad, T. Nakae, H. Nikaido, Permeability of Escherichia coli and Salmonella typhimurium cell wall to Oligosaccharides, Fed. Proc. 33 (1974) 1240.

[29] H. Prochnow, V. Fetz, S.K. Hotop, M.A. García-Rivera, A. Heumann, M. Brönstrup, Subcellular quantification of uptake in gram-negative bacteria, Anal. Chem. 91 (2019) 1863–1872, https://doi.org/10.1021/acs.analchem.8b03586.

[30] R. Iyer, M.A. Sylvester, C. Velez-Vega, R. Tommasi, T.F. Durand-Reville, A.A. Miller, Whole-cell-based assay to evaluate structure permeation relationships for carbapenem passage through the Pseudomonas aeruginosa porin OprD, ACS Infect. Dis. 3 (2017) 310–319, https://doi.org/10.1021/acsinfecdis.6b00197.

[31] J.D. Prajapati, C.J. Fernández Solano, M. Winterhalter, U. Kleinekathöfer, Characterization of ciprofloxacin permeation pathways across the porin OmpC using metadynamics and a string method, J. Chem. Theor. Comput. 13 (2017) 4553–4566, https://doi.org/10.1021/acs.jctc.7b00467.

[32] S. Acosta-Gutiérrez, L. Ferrara, M. Pathania, M. Masi, J. Wang, I. Bodrenko, M. Zahn, M. Winterhalter, R.A. Stavenger, J.M. Pagès, J.H. Naismith, B. Van Den Berg, M.G.P. Page, M. Ceccarelli, Getting drugs into gram-negative bacteria: rational rules for permeation through general porins, ACS Infect. Dis. 4 (2018) 1487–1498, https://doi.org/10.1021/acsinfecdis.8b00108.

[33] K.R. Pothula, C.J.F. Solano, U. Kleinekathöfer, Simulations of outer membrane channels and their permeability, Biochim. Biophys. Acta Biomembr. 1858 (2016) 1760–1771, https://doi.org/10.1016/j.bbamem.2015.12.020.

[34] C.F. Sousa, J.T.S. Coimbra, I. Gomes, R. Franco, P.A. Fernandes, P. Gameiro, The binding of free and copper-complexed fluoroquinolones to OmpF porins: an experimental and molecular docking study, RSC Adv. 7 (2017) 10009–10019, https://doi.org/10.1039/C6RA26466B.

[35] G.M. Decad, H. Nikaido, Outer membrane of gram negative bacteria. XII. Molecular sieving function of cell wall, J. Bacteriol. 128 (1976) 325–336.

[36] R. O'Shea, H.E. Moser, Physicochemical properties of antibacterial compounds: implications for drug discovery, J. Med. Chem. 51 (2008) 2871–2878, https://doi.org/10.1021/jm700967e.

[37] D.G. Brown, T.L. May-Dracka, M.M. Gagnon, R. Tommasi, Trends and exceptions of physical properties on antibacterial activity for gram-positive and gram-negative pathogens, J. Med. Chem. 57 (2014) 10144–10161, https://doi.org/10.1021/jm501552x.

[38] J. Vergalli, I.V. Bodrenko, M. Masi, L. Moynié, S. Acosta-Gutiérrez, J.H. Naismith, A. Davin-Regli, M. Ceccarelli, B. van den Berg, M. Winterhalter, M. Pagès, Porins and small- molecule translocation across the outer membrane of Gram-negative bacteria, Nat. Rev. Microbiol. 18 (2019) 164–176, https://doi.org/10.1038/s41579-019-0294-2.

[39] R.B. Van Breemen, Y. Li, Caco-2 cell permeability assays to measure drug absorption, Expet Opin. Drug Metabol. Toxicol. 1 (2005) 175–185, https://doi.org/10.1517/17425255.1.2.175.

[40] P. Berben, A. Bauer-Brandl, M. Brandl, B. Faller, G.E. Flaten, A.C. Jacobsen, J. Brouwers, P. Augustijns, Drug permeability profiling using cell-free permeation tools: overview and applications, Eur. J. Pharmaceut. Sci. 119 (2018) 219–233, https://doi.org/10.1016/j.ejps.2018.04.016.

[41] R. Tommasi, R. Iyer, A.A. Miller, Antibacterial drug discovery: some assembly required, ACS Infect. Dis. 4 (2018) 686–695, https://doi.org/10.1021/acsinfecdis.8b00027.

[42] F. Graef, R. Richter, V. Fetz, X. Murgia, C. De Rossi, N. Schneider-Daum, G. Allegretta, W. Elgaher, J. Haupenthal, M. Empting, F. Beckmann, M. Brönstrup, R. Hartmann, S. Gordon, C.M. Lehr, In vitro model of the gram-negative bacterial cell envelope for investigation of anti-infective permeation kinetics, ACS Infect. Dis. 4 (2018) 1188–1196, https://doi.org/10.1021/acsinfecdis.7b00165.

[43] O. Lieleg, K. Ribbeck, Biological hydrogels as selective diffusion barriers, Trends Cell Biol. 21 (2011) 543–551, https://doi.org/10.1016/j.tcb.2011.06.002.

[44] K.M. Wheeler, G. Cárcamo-Oyarce, B.S. Turner, S. Dellos-Nolan, J.Y. Co, S. Lehoux, R.D. Cummings, D.J. Wozniak, K. Ribbeck, Mucin glycans attenuate the virulence of Pseudomonas aeruginosa in infection, Nat. Microbiol. 4 (2019) 2146–2154, https://doi.org/10.1038/s41564-019-0581-8.

[45] O. Smithies, Zone electrophoresis in starch gels: group variations in the serum proteins of normal human adults, Biochem. J. 61 (1955) 629–641, https://doi.org/10.1042/bj0610629.

[46] R. Bachvaroff, P.R.B. McMaster, Region of rapidly, Science (80-.) 143 (1964) 1177–1179, https://doi.org/10.1126/science.143.3611.1177.

[47] G.H. Lathe, C.R. Ruthven, Separation of substances and estimation of their relative molecular sizes by the use of columns of starch in water, Biochem. J. 62 (1956) 665–674, https://doi.org/10.1042/bj0620665.

[48] W.A.M. Elgaher, K.K. Sharma, J. Haupenthal, F. Saladini, M. Pires, E. Real, Y. Mély, R.W. Hartmann, Discovery and structure-based optimization of 2-Ureidothiophene-3-carboxylic acids as dual bacterial RNA polymerase and viral reverse transcriptase inhibitors, J. Med. Chem. 59 (2016) 7212–7222, https://doi.org/10.1021/acs.jmedchem.6b00730.

[49] W.A.M. Elgaher, M. Fruth, M. Groh, J. Haupenthal, R.W. Hartmann, Expanding the scaffold for bacterial RNA polymerase inhibitors: design, synthesis and structure-activity relationships of ureido-heterocyclic-carboxylic acids, RSC Adv. 4 (2014) 2177–2194, https://doi.org/10.1039/c3ra45820b.

[50] A. Liaw, M. Wiener, Classification and regression by randomForest, R. News 2 (2002) 18–22, https://doi.org/10.1002/sres.1082.

[51] A.H. Delcour, Outer membrane permeability and antibiotic resistance, Biochim. Biophys. Acta 1794 (2009) 808–816, https://doi.org/10.1016/j.bbapap.2008.11.005.Outer.

[52] K.J. Williams, L.J.V. Piddock, Accumulation of rifampicin by Escherichia coli and Staphylococcus aureus, J. Antimicrob. Chemother. 42 (1998) 597–603, https://doi.org/10.1093/jac/42.5.597.

[53] M. Vaara, Comparative activity of rifabutin and rifampicin against Gram-negative bacteria that have damaged or defective outer membranes, J. Antimicrob. Chemother. 31 (1993) 799–801.

[54] B. Amsden, Solute diffusion within hydrogels. Mechanisms and models, Macromolecules 31 (1998) 8382–8395, https://doi.org/10.1021/ma980765f.

[55] E. Axpe, D. Chan, G.S. Offeddu, Y. Chang, D. Merida, H.L. Hernandez, E.A. Appel, A multiscale model for solute diffusion in hydrogels, Macromolecules 52 (2019) 6889–6897, https://doi.org/10.1021/acs.macromol.9b00753.

[56] S. Wang, C. Li, L. Copeland, Q. Niu, S. Wang, Starch Retrogradation : A Comprehensive Review vol. 14, 2015, https://doi.org/10.1111/1541-4337.12143.

[57] C. Siviello, F. Greco, D. Larobina, Analysis of the aging effects on the viscoelasticity of alginate gels, Soft Matter 12 (2016) 8726–8735, https://doi.org/10.1039/c6sm01671e.

[58] J. Alemán, A.V. Chadwick, J. He, M. Hess, K. Horie, R.G. Jones, P. Kratochvíl, I. Meisel, I. Mita, G. Moad, S. Penczek, R.F.T. Stepto, Definitions of terms relating to the structure and processing of sols, gels, networks, and inorganic-organic hybrid materials (IUPAC recommendations 2007), Pure Appl. Chem. 79 (2007) 1801–1829, https://doi.org/10.1351/pac200779101801.

[59] K. Phan, T. Ferenci, The fitness costs and trade-off shapes associated with the exclusion of nine antibiotics by OmpF porin channels, ISME J. 11 (2017) 1472–1482, https://doi.org/10.1038/ismej.2016.202.

[60] I. Chopra, M. Roberts, Tetracycline Antibiotics : mode of action , applications , molecular biology , and epidemiology of bacterial resistance, Microbiol. Mol. Biol. Rev. 65 (2001) 232–260, https://doi.org/10.1128/MMBR.65.2.232.

[61] Y. Someya, A. Yamaguchi, T. Sawai, A novel glycylcycline, 9-(N,N-dimethylglycylamido)-6-demethyl-6- deoxytetracycline, is neither transported nor recognized by the transposon Tn10-encoded metal-tetracycline/H+ antiporter, Antimicrob. Agents Chemother. 39 (1995) 247–249, https://doi.org/10.1128/aac.39.1.247.

[62] M.F. Richter, P.J. Hergenrother, The challenge of converting gram-positive-only compounds into broad-spectrum antibiotics, Ann. N. Y. Acad. Sci. 1435 (2019) 18–38, https://doi.org/10.1111/nyas.13598.

[63] F. Ruggiu, S. Yang, R.L. Simmons, A. Casarez, A.K. Jones, C. Li, J.M. Jansen, H.E. Moser, C.R. Dean, F. Reck, M. Lindvall, Size matters and how you measure it: a gram-negative antibacterial example exceeding typical molecular weight limits, ACS Infect. Dis. 5 (2019) 1688–1692, https://doi.org/10.1021/acsinfecdis.9b00256.

[64] H. Nikaido, Porins and specific diffusion channels in bacterial outer membranes, J. Biol. Chem. 269 (1994) 3905–3908.

[65] H.I. Zgurskaya, C.A. Löpez, S. Gnanakaran, Permeability barrier of gram-negative cell envelopes and approaches to bypass it, Physiol. Behav. 1 (2015) 512–522, https://doi.org/10.1016/j.physbeh.2017.03.040.

[66] S.J. Cooper, G. Krishnamoorthy, D. Wolloscheck, J.K. Walker, V.V. Rybenkov, J.M. Parks, H.I. Zgurskaya, Molecular properties that define the activities of antibiotics in Escherichia coli and Pseudomonas aeruginosa, ACS Infect. Dis. 4 (2018) 1223–1234, https://doi.org/10.1021/acsinfecdis.8b00036.

[67] E.N. Parker, B.S. Drown, E.J. Geddes, H.Y. Lee, N. Ismail, G.W. Lau, P.J. Hergenrother, Implementation of permeation rules leads to a FabI inhibitor with activity against Gram-negative pathogens, Nat. Microbiol. (2019) 1–9, https://doi.org/10.1038/s41564-019-0604-5.

[68] M. Widya, W.D. Pasutti, M. Sachdeva, R.L. Simmons, P. Tamrakar, T. Krucker, D.A. Six, Development and optimization of a higher-throughput bacterial compound accumulation assay, ACS Infect. Dis. 5 (2019) 394–405, https://doi.org/10.1021/acsinfecdis.8b00299.

[69] X. Tabary, N. Moreau, C. Dureuil, F. Le Goffic, Effect of DNA gyrase inhibitors pefloxacin, five other quinolones, novobiocin, and clorobiocin on Escherichia coli topoisomerase I, Antimicrob. Agents Chemother. 31 (1987) 1925–1928, https://doi.org/10.1128/AAC.31.12.1925.

[70] World Health Organization,, Prioritization of Pathogens to Guide Discovery, Research and Development of New Antibiotics for Drug Resistant Bacterial Infections, Including Tuberculosis, WHO/EMP/IAU/2017.12, 2017.

[71] European Committee on Antimicrobial Susceptibility Testing, EUCAST, 2020. https://mic.eucast.org/Eucast2. (Accessed 7 April 2020). https://mic.eucast.org/Eucast2/